Slicing Using a Conventional Velocity Map Imaging Setup: O_2, I_2, and I_2^+ Photodissociation[†]

Dmitri A. Chestakov, Shiou-Min Wu, Guorong Wu,[‡] and David H. Parker*

Department of Molecular and Laser Physics, University of Nijmegen, Toernooiveld 1, 6525ED, Nijmegen, The Netherlands

André T. J. B. Eppink

School of Chemistry, University of Leeds, Leeds LS2 9JT, U.K.

Theofanis N. Kitsopoulos

Department of Chemistry, University of Crete and Institute of Electronic Structure and Laser (IESL), Foundation for Research and Technology−Hellas (FORTH), P.O. Box 1527, 711 10 Heraklion-Crete, Greece

Received: February 27, 2004; In Final Form: May 3, 2004

The combination of a standard velocity map imaging setup with three different slicing methods is demonstrated for the dissociation of $O_2(X^3\Sigma_g^-)$ ($v = 0$) at 157 nm leading to the $O(^1D) + O(^3P)$ channel, and $I_2(X^1\Sigma_g)$ ($v = 0-4$) at 490 nm leading to the $I(^2P_{3/2}) + I(^2P_{1/2})$ channel. The kinetic energy and angular distributions of the products are compared with the results from conventional (nonsliced) velocity mapping. In addition, one of the methods is applied for the study of field-free dissociation of molecular iodine ion I_2^+ by two-photon excitation at 522 nm.

Introduction

Soloman and Bersohn introduced the first, and most elegant, photofragment imaging method almost 40 years ago.[1] They detected a full three-dimensional (3-D) photofragment *angular* distribution by observing chemical etching on the inside of a coated glass sphere. Chandler and Houston[2] made the next major step with ion imaging, which was followed later by a higher resolution variant called velocity map imaging.[3] This imaging technique[4] captures a two-dimensional (2-D) projection of the 3-D *speed and angular* distribution of photofragments. A mathematical inversion procedure recovers the 3-D information from the 2-D projection.[5] In some cases this procedure is invalid due to product alignment effects[6] or to an inhomogeneous flux-to-density transformation,[7] or it is just too noisy; alternative experimental methods have thus been introduced which "slice" out the desired information directly from the 3-D distribution. Slicing also can improve the image signal-to-background ratio, as illustrated in this paper. We describe photodissociation studies of O_2, I_2, and I_2^+ using three simple "slicing" methods which, unlike previous methods, require no modification of the standard velocity map imaging apparatus.

A typical imaging apparatus[3] is shown schematically in Figure 1. ⊗ marks the crossing of a pulsed molecular beam and laser beams between the repeller (R) and extractor (E) electrodes. Photodissociation takes place, creating a set of expanding Newton spheres of neutral fragment molecules. Immediately after their formation the neutral species are state-selectively ionized using REMPI (resonance enhanced multiphoton ioniza-
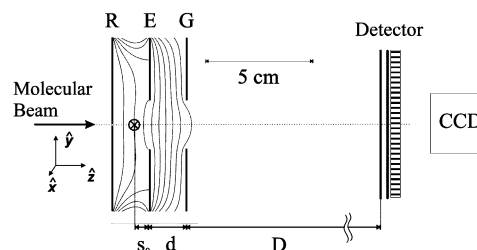
Figure 1. Imaging apparatus showing repeller, extractor, and ground electrodes and electrostatic potential lines. At ⊗ the molecular beam crosses the counterpropagating dissociation and ionization lasers. $s_0 = 5$ mm, $d = 15$ mm, $D = 370$ mm, and the detector diameter is 40 mm.

tion) by a second, counterpropagating laser beam, converting the neutral Newton spheres to ionic spheres with negligible effects on their original angle−speed distributions. Open electrodes (repeller, extractor, and ground (G)) create an electrostatic lens that crushes the ion spheres in the time-of-flight tube direction and maps ions of the same velocity (speed and angle) to the same point onto a 2-D position sensitive detector (PSD), independent of their point of creation. A CCD camera and personal computer monitor the PSD. With the use of velocity map imaging, all origins of the product Newton velocity spheres of the nascent products are superimposed; this greatly enhances the resolution of the method. The challenge is to maintain velocity mapping while obtaining only a center slice of the 3-D ion sphere.

Ion trajectory analysis of the velocity map imaging apparatus[3] has shown that a high repeller plate voltage V_R ensures sufficient "crushing" of the 3-D sphere, so all ions of a given charge/mass ratio arrive at the detector within a few tens of nanoseconds. For example, an arrival time spread $\Delta t_{arrival} \sim 30$ ns was found experimentally[3] for a sphere of O^+ ions with 1.0 eV recoil
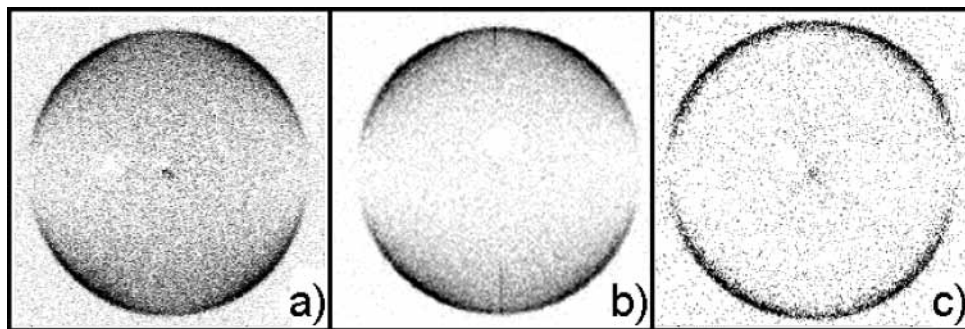
Figure 2. O^+ images from $O(^1D)$ atom products of the photodissociation of O_2 at 157 nm, under (a) full crush, where the background O atoms are also evident, (b) partial slice, and (c) best-slice conditions. Both lasers are polarized parallel to the detector face along the vertical axis in the figure. Darker areas correspond to higher signals.

energy (recoil velocity v_{recoil} = 3473 m/s) and an arrival time $t_{arrival}$ of 1.68 μs, using a flight tube of 370 mm and a repeller electrode voltage, V_R, of 4000 V. $\Delta t_{arrival}$ is a consequence of the ion turn-around time, $t_{turn-around}$, that fragments traveling in the $-z$-direction need to reverse their direction. For a homogeneous field $t_{turn-around}$ is proportional to mv_{recoil} with the ion mass m and the photofragment recoil velocity v_{recoil}; thus "slow and light" ions "crush" more easily than "fast and heavy" ions. Gebhardt et al.[8] and Townsend et al.[9] reported extensive ion trajectory analysis of $\Delta t_{arrival}$ showing that the ion arrival time spread is independent of D, the flight tube length, and follows roughly $\Delta t_{arrival} \propto (KE)^{1/2}/V_R$. For high repeller voltages values of $\Delta t_{arrival}$ < 50 ns are typical.

Delay-line CCD cameras with ∼1 ns time resolution have been used to obtain complete 3-D (x,y,t) velocity mapped images of photofragments under the "typical" conditions described above.[10] The goal of most slicing experiments that use a standard CCD camera is to adjust the apparatus conditions to achieve a longer $\Delta t_{arrival}$ while maintaining velocity map imaging conditions. When $\Delta t_{arrival}$ is long enough, a short (<20 ns) voltage pulse at the detector can be used to selectively record the center of the ion packet. $\Delta t_{arrival}$ can be lengthened by using extra electrodes to extend the region along the ion flight path where acceleration by the electrostatic lens takes place,[9,11] or by letting the Newton sphere expand for a short time before acceleration takes place. The first approach (dc slicing) uses a static electric field while the latter approach uses either an extra grid-covered electrode plus a time delay between ionization and the "turning on" of the electrostatic lens field[8] (delayed extraction), or a time delay between dissociation and ionization[9,12] (optical slicing). A third alternative called one-dimensional optical slicing[13,14] propagates the ionization laser along the z-axis in order to selectively ionize the center portion of the neutral Newton sphere via Doppler selection. This geometry is feasible for crossed-beam scattering but difficult to implement in high-resolution photofragment imaging experiments where the molecular beam also propagates along z. With the optical methods the ion packet is already sliced; thus a narrow detector gate is not necessary.

Experimental Section

The apparatus has been described in detail elsewhere.[3] Briefly, the setup (Figure 1) consists of a pulsed nozzle (General Valve) and skimmer to produce the molecular beam, ion lens system, and multichannel plate (MCP) detector (Burle). The molecular beam of iodine vapor (0.2 Torr) was mixed with argon (1 bar) and introduced into the interaction region along the z-axis through a 2 mm skimmer. To dissociate I_2 at 490 nm, a dye laser (Spectra Physics PDL-2) pumped by the third harmonic of a Nd:YAG laser (Quanta Ray GCR-2A) was used. The

dissociation laser beam (0.5 mJ/pulse) was focused by a *cylindrical* lens (focal length = 24 cm) in the plane orthogonal to the molecular beam. The second (probe) dye laser (Spectra Physics PDL-2) was pumped by the second harmonic of a Nd:YAG laser (Quanta Ray GCR-11). The doubled output (∼304 nm, 0.5 mJ/pulse) was focused by a spherical lens (focal length = 19 cm). Iodine atoms in the $^2P_{1/2}$ state by (2 + 1) REMPI through the $^4D_{1/2}^*$ intermediate state were detected in order to avoid problems with alignment effects that might appear when detecting $^2P_{3/2}$ ground-state iodine atoms. For the experiments with O_2, dissociation by a linearly polarized unfocused 157 nm excimer laser beam (0.3 mJ/pulse) was combined with (2 + 1) REMPI detection of $O(^1D)$ atoms at 205.3 nm using a frequency-tripled dye laser beam (0.5 mJ/pulse) focused by a 20 cm focal length spherical lens onto a molecular beam of neat O_2.

Slicing Methods and Results

One-Lens dc Slicing. As discussed in detail by Townsend et al.,[9] dc slicing with the standard (one-focusing lens) velocity map electrostatic lens is possible with a short detector gate. Using a home-built fast high-voltage switch similar to commercial (Belhke or DEI) switches, we find it is possible to achieve high gain at the front MCP for periods as short as ∼15 ns. We use a dual MCP detector with a center tap between the two MCPs, where the front MCP is pulsed from 0 to −600 V, the center tap is at +300 V, and the back of the second channel plate is at +1200 V. This lower (<800 V) switching voltage allows the use of a one-stage transistor, which is faster than the more common multistage commercial design.

dc slicing requires lower repeller voltages than those used for normal image crushing. Using dc slicing with one focusing lens, it is possible to achieve a value of $\Delta t_{arrival}$ > 200 ns for most fast and heavy (m > ∼12) ions while maintaining V_R > 500 V. The multilens approaches[9,11] achieve larger values of $\Delta t_{arrival}$ for lighter species and allow variation of the final image magnification factor. The advantage of dc slicing is that static fields are used, ensuring a homogeneous electrostatic lens field. One disadvantage is the limited size of the detector. Low values of V_R result in such long arrival times ($t_{arrival} \propto (mV_R)^{1/2}$) that the image size ($\propto v_{recoil}t_{arrival}$) can exceed that of the detector. The most serious drawback of dc slicing is that the low V_R results in a low kinetic energy of the incoming ions, which decreases the ion-to-electron conversion efficiency at the MCP. This problem can only be circumvented by adding an extra grid electrode for postacceleration immediately before the detector.[11]

Raw O^+ images for detection of $O(^1D)$ atoms with 0.39 eV translational energy from photodissociation of O_2 at 157 nm are shown in Figure 2 using a normal "crush" and narrow gate detection (method 1) for two conditions resulting in different

$\Delta t_{\text{arrival}}$ values. In this experiment both the photodissociation and 205.3 nm REMPI probe lasers were linearly polarized along the y-axis, parallel to the detector face. To ensure a full crush (in Figure 2a), $V_R = 1500$ V and a specially tuned "slow" high-voltage switch were used, resulting in constant gain during the experimental arrival time spread $\Delta t_{\text{arrival}} \sim 50$ ns. The partial slice image in Figure 2b was obtained using a 15 ns high-voltage switch with $V_R = 1500$ V, $\Delta t_{\text{arrival}} \sim 50$ ns, and for the minimal slice in Figure 2c, $V_R = 600$ V and $\Delta t_{\text{arrival}} \sim 90$ ns. Analysis of the speed distribution yields results in agreement with the experimental gate width/$\Delta t_{\text{arrival}}$ ratio. The sliced images are of good quality—round, sharp, and homogeneous—as expected for dc slicing conditions. Background is also suppressed (Figure 2b) compared to crushing (Figure 2a) since most of the signal arrives during the wider slice gate while background is more evenly spread in time. The background arises from thermal O_2 molecules in the detection chamber photodissociated along the full length of the (unfocused) 157 nm beam. For the sharpest slice (Figure 2c) more signal is cut away, which lowers the signal-to-background ratio. The image size and flight times increase with decreasing repeller voltage. The sliced image in Figure 2c is larger at the detector than the crushed image, owing to the lower value of V_R. Due to this larger size, a higher ion count rate per laser shot is possible since the probability of overlapping events is decreased. Better slicing can be achieved at even lower repeller voltages, but the size of a single ion event decreases rapidlly below $V_R = 600$ V for oxygen ions, resulting in a large loss of signal compared to CCD chip background.

O_2 excited at 157 nm, near the maximum of the $B^3\Sigma_u^- - X$ $^3\Sigma_g^-$ Schumann—Runge continuum, dissociates to $O(^1D) + O(^3P)$ products with a parallel angular distribution ($\beta = 2$). An exceptionally strong alignment effect observable in the crushed image and quite clear in the sliced images results in a decrease in signal for atoms flying along the laser polarization direction (vertical axis in Figure 2). Wigner—Witmer correlation rules predict that $O(^1D)$ arising from the $B^3\Sigma_u^-$ state should be formed exclusively in $M_J = 0$, in accord with the observed alignment effect.[15] Most striking is that this extremely strong alignment effect occurs at an excess energy of 0.79 eV. One would expect curve-crossing and related processes to lower the product alignment at such a high excess energy, but this is not the case. A full analysis of these images including the effects of the partial crush, $O(^1D)$ alignment, and a Wigner—Witmer type correlation analysis including spin—orbit coupling will be presented later.

Optical Slicing. Optical slicing as demonstrated by Tonokura and Suzuki[12] uses a properly focused probe laser to ionize a slice through the center of the neutral product sphere. Suits and co-workers[9] have also described a "raster" variant of this approach. Both methods are illustrated schematically in panels a and b of Figure 3.

In Figure 3 the ionization laser focus is small compared to the size of the Newton sphere, resulting in slicing, and for illustration in the figure it is Doppler-tuned so that it ionizes neutral fragments moving only along the y-axis with $v_x = 0$. Sources of upward and downward moving velocities are indicated. In all three methods the laser must be scanned across the Doppler profile to collect all velocities (in the *xy* slice plane) equally.

The Suzuki method applies two lasers (photolysis and probe), *both* focused with cylindrical lenses into ribbon shapes, with the flat sheet parallel to the detector face. The thin sheet ionization geometry needed for slicing is also advantageous in velocity map imaging, since the lens magnification factor is slightly dependent on the position (s_0 in Figure 1) along the
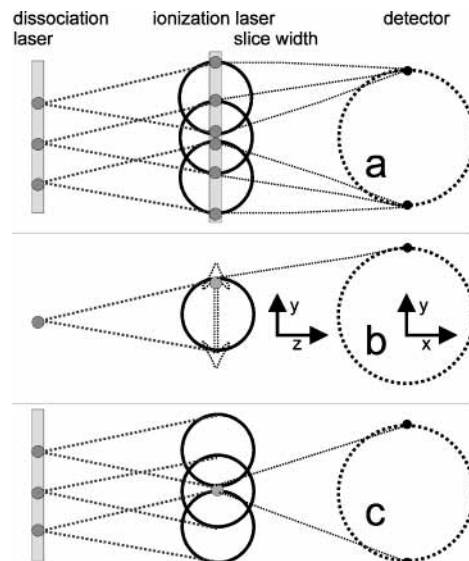
Figure 3. Schematic diagram of optical slicing: (a) the "sheet—sheet" method introduced by Suzuki, (b) the "raster" or "dot—dot" method of Suits and co-workers, and (c) our "sheet—dot" variant.

time-of-flight direction.[3] A thin sheet dissociation geometry close to the probe sheet region yields the highest signal levels. The photolysis laser produces an expanding disk-shaped cloud of neutral products moving with v_{beam}, the molecular beam velocity. After a $0.1-2$ μs time delay, τ, the probe laser ionizes at a distance $\Delta z = v_{\text{beam}}\tau$ downstream the middle part of this cloud; i.e., it "slices" the expanding spheres of the products, creating flat rings of ions which are projected onto the detector.

The advantages of optical slicing are in the reduction of space charge and saturation effects, and in the higher degree of slicing. The time delay introduced in optical slicing results in a larger $t = 0$ ion volume than in the other slicing methods, which reduces space charge effects. When using velocity map imaging, the large origin volume is not a problem. The laser flux is also lower when using a cylindrical lens for the dissociation laser, reducing saturation effects. Furthermore, all ions of interest are collected at the detector, which is efficient and allows mass selection by a standard ($\sim$100 ns) high-voltage detector switch. Another important advantage of optical slicing is in the narrow slice width. By paying attention to beam shaping, it is possible to reduce the width of the thin sheet to $\sim$50 μm. The ratio of slice width to sphere width for a 2000 μm neutral Newton sphere diameter is <3% in this case, which is often narrower than slicing using delayed extraction, as described in the next section.

In addition to the "sheet—sheet" method of Suzuki, Suits and co-workers[9] have described a "dot—dot" raster method (Figure 3b) where both the dissociation and probe lasers are focused with spherical lenses. This yields a signal along a horizontal stripe through the sliced image, so the probe laser beam must be repeatedly displaced up and down through the neutral Newton sphere to recover the full image.

In Figure 3c we describe a different variant of optical slicing using a "sheet—dot" geometry where the dissociation laser is focused by a cylindrical lens and the probe laser by a spherical lens. Providing that the dissociation disk is much larger along the y-axis than the ionization line, all nascent velocity is fed into the probe beam position. This makes extreme use of velocity map imaging since none of the mapped velocities arise from the same point in space. Using sheet—dot slicing, the entire slice is captured without displacing the probe laser beam. For difficult $(2 + 1)$ REMPI the higher flux of the "dot" focused probe laser

Conventional Velocity Map Imaging Setup for Slicing

J. Phys. Chem. A, Vol. 108, No. 39, 2004 **8103**

can yield signal under conditions where a cylindrically focused "sheet" laser beam cannot.

The "sheet–sheet" and "sheet–dot" geometry of optical slicing can show a bias against products with high recoil velocities, especially those products traveling along the y-axis, perpendicular to the molecular–laser beam plane. The center slice of the moving Newton sphere is probed by setting $\Delta z/\tau = v_{beam}$. To ionize the neutral particles traveling up–down (for a horizontal time-of-flight tube), it is necessary that particles with positive y recoil velocity v_{recoil} are produced at a distance $d = v_{recoil}\tau$ below the probe laser focus. This distance cannot exceed the molecular beam radius, typically $\sim$1 mm, meaning that for a typical $\tau = 500$ ns, particles with recoil velocities above 2000 m/s will be missed in the "sheet–dot" geometry and less efficiently detected in the "sheet–sheet" geometry.

Similar slicing approaches have been used in crossed molecular beam measurements using unskimmed beams, where the reaction products are formed in an extended region much larger than the "dot" focus of the probe laser.[16] In that case the probe laser delay is scanned in order to let all products fly through the probe laser region.

Delayed Extraction. Delayed extraction by electric field switching is a standard method in photofragment time-of-flight velocity analysis.[17] Photodissociation and fragment ionization occurs field-free, and the expanding ion cloud is pushed toward the MCP detector by high voltage applied 200–800 ns after the probe laser pulse. We address here the conditions needed to avoid distortions with the open-lens electrodes used in velocity mapping. Kitsopoulos and co-workers[8] circumvented the open lens problem by including an extra grid-covered electrode used for the field pulsing. With an ultrafine (40 lines/mm) mesh this grid electrode does not measurably distort the image, and it allows slicing of light ions such as H$^+$,[18] which are not yet possible with dc slicing.

To obtain distortion-free images in experiments combining open electrodes and delayed extraction, we found it necessary to connect two independent and similar high-voltage (<5 kV) switches to the repeller and extractor electrodes. Unsuccessful attempts were made to switch only one electrode in order to change quickly from field-free to velocity mapping conditions. This is probably due to the difficulty in finding the perfect balance of voltages on the repeller and the open extractor electrode before pulsing. Attempts to connect both electrodes using a voltage divider and one high-voltage switch did not give stable results. Good quality well-sliced images using time delays up to $\tau = 2$ μs could be obtained using two identical switches with nanosecond control on the individual switching times. Two switches are necessary due to oscillations on the 10–50 ns time scale specific to each electrode due to reactive impedance (electrode capacitance, induction of the wires, etc). By adjusting the relative timing of the pulses, it is possible to minimize the effect of the oscillations. In this configuration a wide range of ion arrival time spreads, $\Delta t_{arrival}$, can be reached, depending on τ, the switching time delay. As in method 1, a fast detector switch slices out the middle of the ion package.

Comparison of Optical "Sheet–Dot" and Delayed Extraction with Crush Inversion. One-lens dc slicing is compared with normal (crush invert) imaging in Figure 2, for O$_2$ photodissociation producing fast (2210 m/s) O atoms, an experiment in the "heavy and fast" limit. Near-threshold photodissociation of I$_2$ around 500 nm, a system with much lower product recoil, was also studied. Due to the very low product kinetic energy, one-lens dc slicing was not applicable. This is a "heavy but slow" case where an extremely low repeller
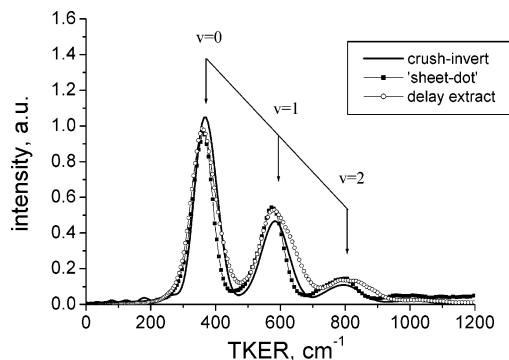
Figure 4. Total kinetic energy distributions of iodine ions, obtained by different methods. Three peaks correspond to the 490 nm dissociation of I$_2$(X$^1\Sigma_g$) ($v = 0$, 1, 2) states to the second dissociation limit (I(^{2}P$_{3/2}$) + I (^{2}P$_{1/2}$)).
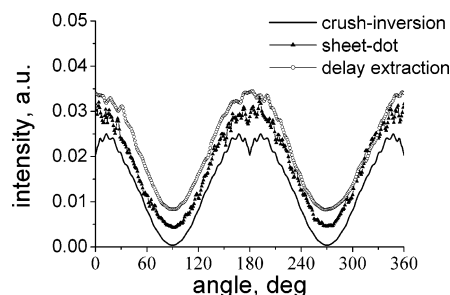
Figure 5. Angular distributions for I$_2$(X$^1\Sigma_g$) ($v = 0$) dissociation channel, obtained by different methods. To aid comparison, the upper curves have been shifted vertically by 0.005 arbitrary units.

voltage is necessary to obtain $\Delta t_{arrival} > \sim$80 ns. The resulting I$^+$ kinetic energy is too low to be detected by the MCP.

Optical and delayed extractions are applicable, however, as shown in Figure 4, where velocity distributions obtained from a crushed inverted image are compared with those from sheet–dot and delayed extraction images for I$^+$ from I ^{2}P$_{1/2}$ atomic products of I$_2$ photodissociation at 490 nm. Three peaks are seen corresponding to photodissociation of different vibrational levels of ground-state I$_2$ in the $v = 0$, 1, and 2 which are populated in the molecular beam.

The kinetic energy distributions from both optical and delayed extraction slicing are similar to the crush-inversion results. Optical slicing yields slightly more narrow peaks than both delayed extraction and the crush-inversion method. For the crushed and delayed extraction methods space charge can result in peak broadening of 2–4% when there are as few as $\sim$10 ions in the $\sim$100 μm focus region. This includes *all* ions, especially those not detected, and thus space charge can easily be a limiting factor in the peak width. The width of the peaks is also sensitive to the rotational energy distribution of the parent molecules, as shown previously[19] for IBr dissociation. One can estimate that in our experiment the rotational broadening adds $\sim$6% to the iodine ion velocity, assuming $T_{rot} \sim$ 20 K for the molecular beam.

Another sensitive test of the quality of the sliced images is the accuracy and reproducibility of the angular distribution. The experiments were repeated over a period of several months, each time with different experimental conditions, and the results were compared. For one set of data the angular distributions for the $v = 0$ peak (see Figure 4) are shown in Figure 5. As is usual for inversion algorithms, some noise is created at 0° and 180° in the data for crush inversion.

The angular distributions were fitted to a $(1 + \beta P(\cos(\theta))$ function.[20] The resulting values for β are presented in (Table

8104 *J. Phys. Chem. A, Vol. 108, No. 39, 2004*

Chestakov et al.

TABLE 1: Anisotropy Parameter β of the Angular Distribution of Iodine Atoms from I_2 Photodissociation at 490 nm, Measured by Different Slicing Methods

method	β-parameter[a]
crush invert	1.86 ± 0.02
sheet−dot	1.85 ± 0.06
delay extract	1.89 ± 0.02

[a] Uncertainty limits represent one standard deviation for a set of ~40 different measurements.
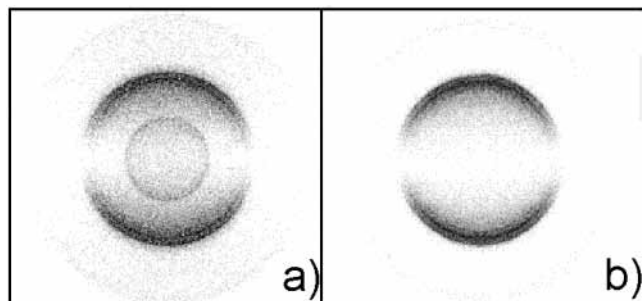
Figure 6. I^+ images for two-photon dissociation of $I_2^+(X^2\Pi_{3/2g})$ ion at 522 nm laser light (a) 30 ns and (b) 1 μs after ion formation. The I_2^+ ions were formed by $(2 + 1)$ REMPI of I_2 molecules using 331 nm laser light. Both laser polarizations lie along the vertical axis of the images.

1). While β from the three methods agrees within the uncertainty, the reproducibility is lowest for the "sheet−dot" method, due mainly to difficulties in ensuring a homogeneous dissociation laser sheet.

Zero-Field Molecular Ion Photodissociation. An additional advantage of delayed extraction is its applicability where field-free conditions are needed, such as crossed-beam studies of *ion−ion* or *ion−neutral* reactions. Weisshaar and co-workers[21] have reported such an experiment using standard high-voltage switching for delayed extraction. The present study examines the optimal switching conditions for this type of measurement. After the molecular ions have been formed, they are allowed to drift with the molecular beam for microseconds, simulating the time needed for collisions with particles from another molecular beam. The electric field is then switched on and the decrease in signal in the resulting image (which can be crushed or sliced) is evaluated.

To simulate an ion collision experiment, a sample of I_2^+ molecular ions was prepared in a molecular beam of I_2 in argon by $(2 + 1)$ REMPI via the $[^2\Pi_{3/2}]5d;1g$ state at 331.01 nm. The I_2^+ was photodissociated using a second, slightly focused laser beam at 522 nm at varying time delays afterward, after which the repeller−extractor fields were switched on using identical high-voltage switches. The resulting raw I^+ images are shown in Figure 6 for a 30 (Figure 6a) or 1000 ns (Figure 6b) time delay between formation and photodissociation. Analysis of the photoelectron image for the REMPI process shows that the I_2^+ ions are formed predominately in the $X^2\Pi_{3/2g}$ spin−orbit state. The sharp rings in the middle of the I^+ image arise from two-photon dissociation of I_2^+ to the $[I^+(^1D) + I(^3P_2)]$ and the $[I^+(^3P_0) + I(^2P_{1/2})]$ limits. In Figure 6a both laser beams overlap in space, while in Figure 6b the ionization laser is moved upstream in the molecular beam to a position where the signal from the dissociation laser is optimized. The I_2^+ formation laser also creates a small amount of I^+ signal, such as the small ring in the middle of Figure 6a; this disappears for larger spatial separations of the two laser beams. The intensity of the dissociation laser signal in both images is the same, showing that after 1 μs the molecular ion package can be still kept in

molecular beam without losses. This method is thus useful for ion collision studies, and for studying the photodissociation of isolated molecular ions formed by REMPI.

Discussion

Three different approaches were shown for slicing using a standard velocity map imaging apparatus. We studied O_2 dissociation at 157 nm, I_2 dissociation at 490 nm, and I_2^+ dissociation at 522 nm. Sliced images using each method were analyzed and compared with each other and with standard "crushing". For "heavy and fast" ions the simplest approach is one-lens dc slicing, which yields moderately sliced images and improved signal-to-background ratios. For "heavy ($m > \sim 12$) but slow" ions from threshold photodissociation, optical slicing is the most attractive due to diminished space charge problems, but delayed extraction is competitive and simpler to implement, especially for small photodissociation cross sections where the cylindrical lens in "sheet−dot" slicing can result in a too-low laser flux.

All three of the methods can be used without changing the standard velocity map imaging apparatus. Although the addition of an extra electrode improves the operating velocity range of dc slicing in a very simple modification of the velocity map imaging apparatus, the original delayed extraction method using a fine-grid electrode is at present the most versatile over the widest ranges of product mass and velocity. An ultimate remaining challenge for all slicing methods is the slicing of a Newton sphere of photoelectrons. This will require delayed extraction and a much faster detection gate than those used in conventional velocity mapping.

References and Notes

(1) Soloman, J. *J. Chem. Phys.* **1967**, *47*, 889. Soloman, J.; Chandra, P.; Jonah, C.; Bersohn, R. *J. Chem. Phys.* **1971**, *55*, 1908.

(2) Chandler, D. W.; Houston, P. L. *J. Chem. Phys.* **1987**, *87*, 1445.

(3) Eppink, A. T. J. B.; Parker, D. H. *Rev. Sci. Instrum.* **1997**, *68*, 3477.

(4) *Imaging in Molecular Dynamics, Technology and Applications*; Whitaker, B. J., Ed.; Cambridge University Press: Cambridge, 2003.

(5) Eppink, A. T. J. B.; Wu, S.-M.; Whitaker, B. J. In *Imaging in Molecular Dynamics, Technology and Applications*; Whitaker, B. J., Ed.; Cambridge University Press: Cambridge, 2003; pp 65−112.

(6) Rakitzis, T. P. *Chem. Phys. Lett.* **2001**, *342*, 121, and references therein.

(7) Shiu, W.; Lin, J. J.; Liu, K.; Wu, M.; Parker, D. H. *J. Chem. Phys.* **2004**, *120*, 117.

(8) Gebhardt, C. R.; Rakitzis, T. P.; Samartzis, P. C.; Ladopoulos, V.; Kitsopoulos, T. N. *Rev. Sci. Instrum.* **2001**, *72*, 3848.

(9) Townsend, D.; Minitti, M. P.; Suits, A. G. *Rev. Sci. Instrum.* **2003**, *74*, 2530.

(10) Dinu, L.; Eppink, A. T. J. B.; Rosca-Pruna, F.; Offerhaus, H. L.; van der Zande, W. J.; Vrakking, M. J. J. *Rev. Sci. Instrum.* **2002**, *73*, 4206.

(11) Lin, J. J.; Zhou, J.; Shiu, W.; Liu, K. *Rev. Sci. Instrum.* **2003**, *74*, 2495.

(12) Tonokura, K.; Suzuki, T. *Chem. Phys. Lett.* **1994**, *224*, 1.

(13) Kinugawa, T.; Arikawa, T. *J. Chem. Phys.* **1992**, *96*, 4801.

(14) Lorenz, K. T.; Chandler, D. W.; Barr, J. W.; Chen, W. W.; Barnes, G. L.; Cline, J. I. *Science* **2001**, *293* (5537), 2063.

(15) Eppink, A. T. J. B.; Buijsse, B.; Janssen, M. H. M.; van der Zande, W. J.; Parker, D. H. *J. Chem. Phys.* **1998**, *108*, 1305.

(16) Toomes, R. L.; Kitsopoulos, T. N. *Phys. Chem. Chem. Phys.* **2003**, *5*, 2481.

(17) Young, M. A. *J. Chem. Phys.* **1995** *102*, 7925, and references therein.

Conventional Velocity Map Imaging Setup for Slicing

J. Phys. Chem. A, Vol. 108, No. 39, 2004 **8105**

(18) Toomes, R. L.; Samartzis, P. C.; Rakitzis, T. P.; Kitsopoulos, T. N. *Chem. Phys.* **2004**, *301*, 209.

(19) Wrede, E.; Laubach, S.; Schulenburg, S.; Orr-Ewing, A. J.; Ashfold, M. N. R. *Chem. Phys. Lett.* **2000**, *326*, 22.

(20) Zare, R. N. *Angular Momentum, Understanding Spatial Aspects in Chemistry and Physics*; John Wiley and Sons: New York, 1988.

(21) Reichert, E. L.; Thurau, G.; Weisshaar, J. C. *J. Chem. Phys.* **2002**, *117*, 653.